Analysis of Classical Root-Finding Methods Applied to Digital Maximum Power Point Tracking for Sustainable Photovoltaic Energy Generation

Seunghyun Chun, *Student Member, IEEE*, and Alexis Kwasinski, *Member, IEEE*

Abstract—This paper examines the application of various classical root-finding methods to digital maximum power point tracking (DMPPT). An overview of root-finding methods such as the Newton Raphson method , Secant method , bisection method, regula falsi method, and a proposed modified regula falsi method (MRFM) applied to photovoltaic (PV) applications is presented. These methods are compared among themselves. Some of their features are also compared with other commonly used maximum power point (MPP) tracking methods. Issues found when implementing these root-finding methods based on continuous variables in a digital domain are explored. Some of these discussed issues include numerical stability, digital implementation of differential operators, and quantization error. Convergence speed is also explored. The analysis is used to provide practical insights into the design of a DMPPT based on classical root-finding algorithms. A new DMPPT based on an MRFM is proposed and used as the basis for the discussion. It is shown that this proposed method is faster than the other discussed methods that ensure convergence to the MPP. The discussion is approached from a practical perspective and also includes theoretical analysis to support the observations. Extensive simulation and experimental results with hardware prototypes verify the analysis.

Index Terms—Boost converter, maximum power point tracking, microcontroller, optimization, photovoltaics (PVs), renewable energy, variable step size.

I. INTRODUCTION

THIS PAPER discusses the application of classical mathematical root-finding optimization methods for maximum power point tracking (MPPT) of photovoltaic (PV) systems. Since in this study these methods are implemented digitally, practical issues encountered when digitally implementing a method originally based on a continuous domain are also explored. In particular, this study discusses potential errors inherently caused by digital processes not substantially explored in previous MPPT papers, such as algorithm numerical stability, quantization error, and discretization error analysis.

Other important issues found when power electronic systems are utilized as an interface for a sustainable energy application,

such as choosing the specification for the digital pulsewidth modulation (DPWM) and converter parameters, are also addressed and commented. Also, a new MPPT strategy based on a modified regula falsi method (MRFM) is presented and studied according to the analysis mentioned earlier.

The world's energy demand is projected to increase 1.5% yearly between 2007 and 2030 [1]. Yet, since fossil fuels remain the world's main energy source, there is increased concern on how to address the dilemma of meeting this expected energy demand without affecting the environment. It is expected that increased utilization of sustainable energy sources will help to address this issue [2]. In particular, technical advances in PV energy generation, as one of the main sustainable energy sources, have made it a potentially attractive solution for this issue [3]. However, PV modules' high installation and capital costs still create some barriers that limit their application as a widespread solution that would convert predominately resource-consuming present electric generation sources into a power generation base with sustainable characteristics. Hence, in order to make PV generation a truly attractive sustainable choice that contributes to meet future energy demands, it is necessary to maximize its utilization. In order to obtain the maximum possible power output from PV modules, it is necessary to operate them at their absolute maximum power point (MPP) where the derivative of the output power with respect to the output voltage—i.e., *dP/dV*—is zero. However, PV sources have an output current–voltage (*I–V*) characteristic that is nonlinear and varies with different irradiance, temperature, and load conditions. Our optimization problem and motivation for this study is to track and find this MPP and to force the PV panel to operate at this point in the fastest and more stable way possible.

In recent years, numerous MPPT methods have been developed [4]. The majority of them are based on searching the MPP by utilizing the sign of *dP/dV* as an indication of the search direction. Also, digital implementations of MPPT have gained popularity because of the wide selection and technological advances of low-cost, microcontrollers and digital signal processors (DSPs), which have enabled researchers the freedom to change the control algorithm, without extensively modifying the system hardware platform. All these advantages have encouraged research not only in digital controllers in general applications [5], but also in sustainable systems applications, such as solar power [6], [7], wind power [8], and a thermoelectric battery energy storage system [9]. All of these utilize a DSP to process sampled signals. But a thorough analysis of the previously discussed issues found in errors encountered when designing a

digital maximum power point tracking (DMPPT) system was not provided. Thus, the analysis provided in this paper tackling these issues is relevant when designing and implementing a DMPPT system.

There exist many methods to realize MPPT [10] although these are either a slight modification or a variant of two methods [4], [10], [11]. MPPT methods can be grouped into two major approaches. The first group of methods is based on voltage feedback [11]–[13]. In these methods, a predetermined reference voltage is compared with the PV module voltage in a feedback loop. Voltage feedback methods enable one to choose a desirable operating point for unknown or varying load conditions, but they lead to energy inefficiencies because they are not able to adjust to changing environmental conditions. A modification was done in [14] to change the reference voltage at periodic moments in time by momentarily interrupting the system operation and sampling the PV module open circuit voltage in order to update the reference voltage—usually around 70–80% of the PV module open circuit voltage V_{oc}. A disadvantage of the method in [14] is that energy is wasted during system momentary interruptions. Another problem is that the method in [14] is sensitive to aging and dust accumulation, which leads to the issue that the reference voltage may no longer be taken as 70–80% of V_{oc}.

The second group of methods is the power feedback methods, which are based on calculating the power by sensing the voltage and current generated from the PV module. Then, the majority of the algorithms attempt to keep the ratio dP/dV at zero. The perturb and observe method (P&O) [15]–[17] is a popular technique which is easy to implement digitally. But this method oscillates around the MPP causing energy losses. Also, at rapidly changing conditions the operating point can move away from the MPP. An improved P&O method was presented in [16] to solve this problem but difficulties in choosing threshold values were left unaddressed. In [17], an optimization of the P&O method is presented in which the sampling frequency and the fix step size of the method are optimized to take into consideration the dc-dc converter interface and environmental effects. This optimization minimizes the oscillation around the MPP and prevents the system from failing in a rapidly changing environment. Hence, efficiency and stability of the P&O method are improved. However, this optimized strategy is a complex tuning process that eliminates the simple implementation merit of the P&O method and does not fully eliminate the oscillation problem. The incremental inductance method (INC) presented in [18] is another algorithm with the same objective of keeping $dP/dV = 0$ but uses an incremental and instantaneous relation based on output current and voltage I and V, respectively, equal to $dI/dV + I/V = 0$. It still has the oscillation problem around the MPP and the step size is fixed. Oscillation around the MPP can be reduced with a small step size, but it leads to slow convergence to the MPP. Both the P&O and INC methods are considered as an elimination method or a trial and error process. Since both are fixed step size methods, reaching the MPP or convergence is dependent on the initial point of the tracking process and the size of the step. In most cases, if, in an attempt to reach the MPP faster, the step size is too large, both the P&O and INC

methods will oscillate around the MPP. Classical root-finding algorithms are considered iterative interpolation methods with variable step sizes. The use of variable step sizes in root-finding algorithms indicates an inherent fundamental difference with the P&O and INC methods and prevents comparing their convergence speeds in a formal way on equal basis. However, it is possible to identify that owed to their variable step size one advantage of root-finding based algorithms over the P&O and INC methods is that root-finding techniques avoid issues with oscillations. Like the P&O and INC methods, there are many other MPPT algorithms built around the idea of using $dP/dV = 0$, followed by evaluating $dP/dV < 0$ or $dP/dV > 0$ as the decision criterion for the next iteration step of an algorithm. The steepest descent method is widely used and presented in [19]. It is a variable step approach to MPPT that provides convergence speed to MPP close to that of the Newton method approach. However, finding the step size factor is a difficult process and must be tuned for different PV modules. Of particular interest in this study is a newly proposed DMPPT based on a root-finding MRFM. The MRFM is based on the same problem formulation than that specified in other power feedback algorithms: searching for $dP/dV = 0$, yet the approach used here considers the search for $dP/dV = 0$ as a root-finding mathematical problem. The proposed MRFM DMPPT method is well suited for MPPT because root convergence is guaranteed without observing oscillations around the MPP as observed in aforementioned methods. Unlike the optimized P&O [17], the proposed MRFM DMPPT method does not need a complex tuning process and is guaranteed to converge with no oscillation.

In order to provide a complete approach to the discussion and to understand the advantages of the MRFM, this paper explores other MPPT algorithms based on root-finding methods. Thus, it is also relevant to consider applied research in practical optimization techniques to MPPT algorithms [19]–[22]. The method presented in [20] provides a fast convergence in cases where the initial search point is close to the MPP. Yet, it also has the possibility of diverging catastrophically. It also includes the need for calculating not only the first derivative but also the second derivative at any operating point that results in convergence error and accuracy compromises. The recent approach presented in [21] solves the diverging issue in [20] but convergence to the MPP is slow when compared to [19] and [20]. In contrast, the MRFM presented here and in [22] provides a faster convergence to MPP that in [21] which increases the efficiency of energy extraction from PV panels and achieves better performance under varying environmental conditions.

In [23], the effects due to partial shading of the PV panel with tree branches, leaves, or clouds are presented. This causes a decrease in generated power from the PV and also multiple MPPs to occur. In order to present a common comparison approach with other root-finding algorithms, the work presented herein assumes that only a global MPP exists, with no other local MPP present. This approach can still address the aforementioned partial shading issues through hardware by dividing PV arrays and modules into sections, and making each of these sections the input of a multiple-input converter, such as those proposed in [24]–[26]. However, detailed evaluation of the implementation
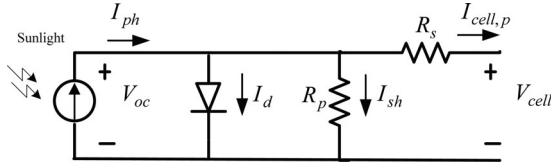
Fig. 1.   Practical PV cell electrical model [27].

of such an approach through multiple-input converters is out of scope of this paper and will be the focus of a future work along with the analysis of root-finding MPP algorithms with local maxima.

This paper is structured as follows. Section II introduces preliminary notions and tools that support and provide context for the analysis. In particular, it discusses the PV modules model. Section III delves into the description of the mathematical basis for the root-finding algorithms that are studied here for MPPT implementation. In particular, this section describes at its ends the MRFM that is newly used here for DMPPT. Section IV discusses the application of classical root-finding algorithms to DMPPT. Section V presents simulation and experimental results comparing each method and its merits are discussed. Preceding analysis is also validated in this Section. Finally, Section VI presents the conclusion of this work.
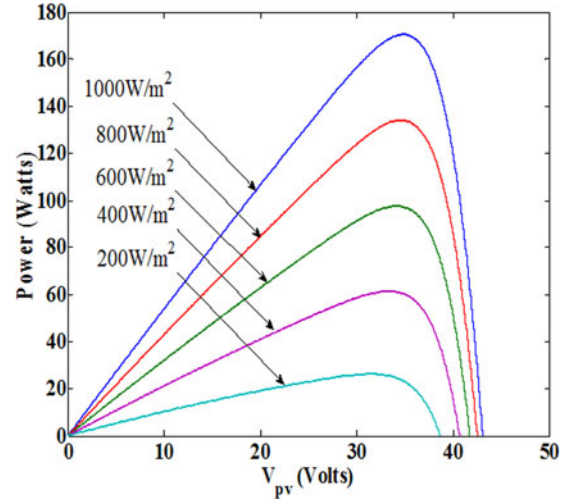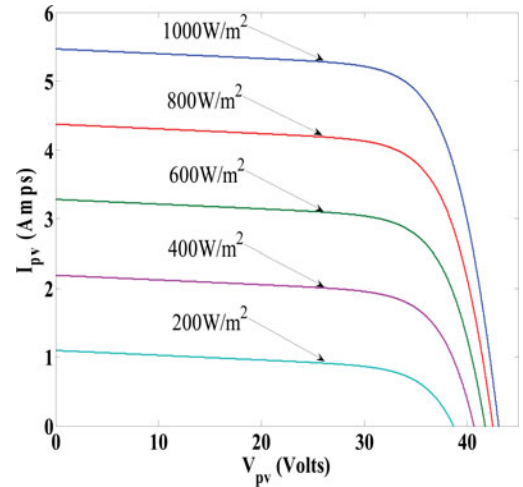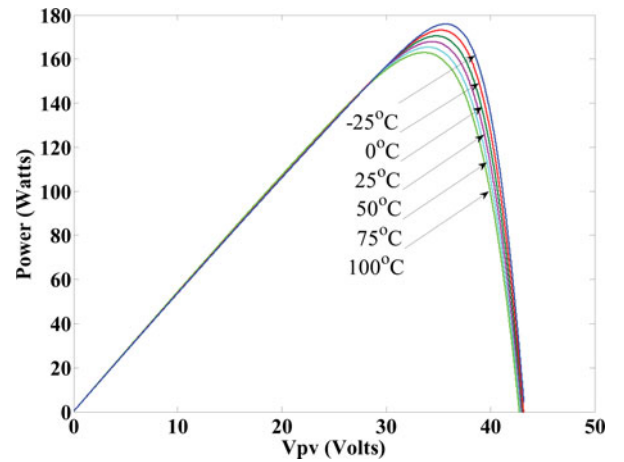
II. Photovoltaic Module Model

Fig. 1 shows a conventional practical model of a PV cell used to provide context for the analysis. This model neglects dynamic effects of self-capacitances. Still, the model is accurate enough as an additional tool to support the discussion but its knowledge is not necessary to realize any of the root-finding algorithms later discussed in this paper. From [27], the PV cell mathematical modeled is given by

$$I_{\text{cell},p} = I_{\text{ph}} - I_s \left(e^{qV_{\text{cell}}/nkT} - 1 \right) - \frac{V_{\text{cell}} + R_s \cdot I_{\text{cell},p}}{R_p}$$

(1)

where $I_{\text{cell},p}$ is the cell output current, I_{ph} is the photocurrent, I_s is the diode saturation current, R_p is the shunt resistance, R_s is the series resistance, q is the electron charge (1.6×10^{-19} C), k is Boltzmann's constant (1.38×10^{-23} J/K), T is the cell's temperature in degree Kelvins, V_{cell} is the output voltage of the cell, and n is a diode scaling constant.

Equation (1) indicates two main factors affecting the PV cell output: temperature and the solar irradiance. The latter dependence is implicitly included in (1), in which I_{ph} is directly proportional to the solar radiation intensity. Since the amount of sunlight depends on the angle of incidence of sun's rays with respect to the panel, it is expected that a PV module's output will vary throughout the day and with weather conditions. As a result of these multiple factors affecting PV modules' output, their power–voltage (P–V) and current–voltage (I–V) characteristics typically show potential for significant variations depending on environmental conditions. Figs. 2–5 exemplify the wide range of possible outputs based on a PV module with the following nominal parameters under the standard testing condition (STC):

Fig. 2.   Irradiance effect on P–V characteristic at constant temperature (25 °C).

Fig. 3.   Irradiance effect on I–V characteristic at constant temperature (25 °C).

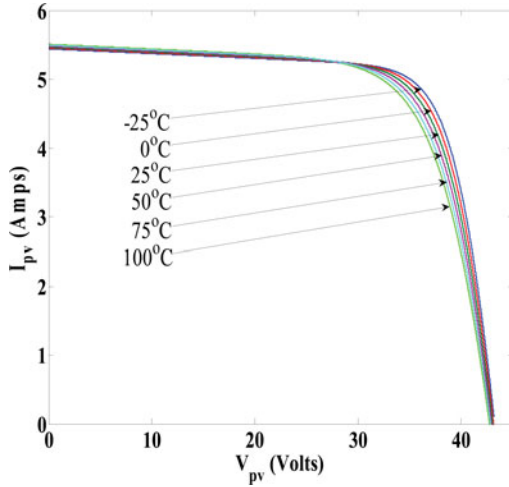Fig. 4.   Temperature effect on P–V characteristic at constant irradiance (1000 W/m^2).

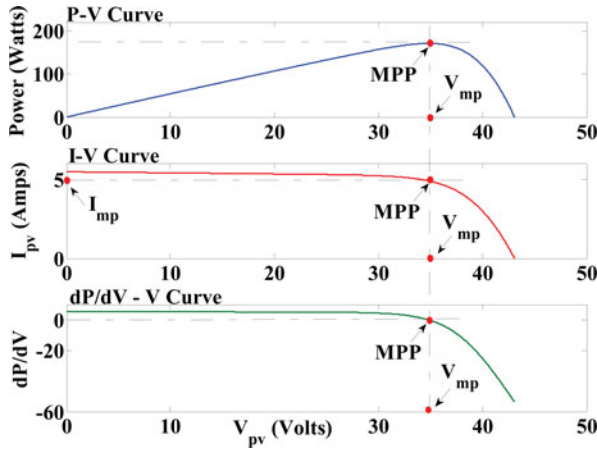Fig. 5. Temperature effect on *I–V* characteristic at constant irradiance $(1000 \, \text{W/m}^2)$.

Fig. 6. Maximum Power Point for different curves of a PV module.

V_{oc}, the open circuit voltage of the module, is 43.2 V, I_{sc}, the short-circuit current of the PV module, is 5.47 A, P_{max}, the maximum power generated, is 170 W, and the corresponding voltage V_{mp} and current I_{mp} are 34.8 V and 4.9 A, respectively. As these figures show, the *I–V* characteristic is nonlinear and varies with different solar irradiance and temperature conditions. Figs. 2 through 5 also indicate that for a given set of conditions (i.e., temperature and solar irradiance) there is an unique operating point for which the output power of the PV module is maximized. This point is called the maximum power point (MPP) and it is achieved for the particular output voltage and current indicated by V_{mp} and I_{mp}, respectively.

Since it is expected that the MPP will vary, it is necessary to implement a control method applied to the power electronic converter interface in order to ensure efficient energy extraction from the PV module. This method is called a maximum power point tracker (MPPT). As Fig. 6 exemplifies, the objective is to track the PV module output to the point where $dP/dV = 0$. The MPPT methods discussed in this paper are classical optimization methods based on a root-finding algorithm. As will be shown in the following sections, these methods provide

an alternative approach to variable step MPPT in most practical settings that may achieve faster MPP tracking compared to fixed step algorithms. These root-finding-based methods, including a newly proposed MRFM, are explained in the next section and their main advantages and disadvantages are compared.

III. ROOT-FINDING ALGORITHMS

Since the problem definition specified in Section II involves finding the MPP—i.e., the point for which the derivative of the output power of a PV module with respect to its output voltage equals zero—it is natural to consider the implementation of conventional root-finding algorithms to solve this problem. One advantage of root-finding MPPT algorithms is that their iterative approach is not a model-based technique, such as [14], in which PV module parameters, such as R_p or R_S, need to be actually identified or implicitly estimated. On the contrary, root-finding algorithms are a completely general approach that search for the zero crossing of a given function—any given function used as the input for the algorithm. Hence, although in this particular case these algorithms are used in a PV application, it is also possible to use the same algorithm in other applications with a physical realization different from the one discussed here, such as finding the MPP of fuel cells. Moreover, since root-finding methods provide the theoretical mathematical basis for solving optimization problems (and finding the MPP is merely a particular optimization problem), these methods constitute the origin of many other MPPT methods [19]–[22]. Some of these algorithms [20], [21] have already been discussed in the past as a possible method to find the point where dP/dV equals zero. Others, such as the MRFM, are new approaches discussed here. Equally important to understanding these methods is to study their similarities and differences. Hence, this section explores these popular root-finding algorithms and compare their performances. Since in these methods the solution is approached through an iterative process, they theoretically require an infinite number of steps to reach the solution with 100% accuracy. In practice, a tolerance condition will determine when the solution is reached. Hence, special attention is paid to evaluating the speed at which each algorithm reaches the tolerated approximation, also known as convergence rate.

A. Open Methods

These methods are initiated with one or two initial approximations of the root. Two well-known open methods will be introduced and also their application to MPPT will be shown.

1) Newton Raphson Method: In order to find a value x^* that is a root of a function $f(x)$—i.e., $f(x^*) = 0$—the Newton Raphson method (NRM) is based on performing an iterative calculation given by

$$x_{n+1} = x_n - \frac{f(x_0)}{f'(x_0)} \quad n = 0, 1, 2 \dots . \tag{2}$$

until $|f(x_n)| \leq \varepsilon$ (where ε is the tolerance). In the NRM, the point x_{n+1} is the root for the tangent line $l_n(x)$ to the function
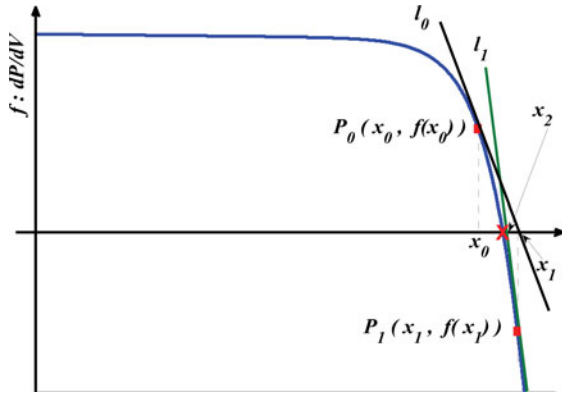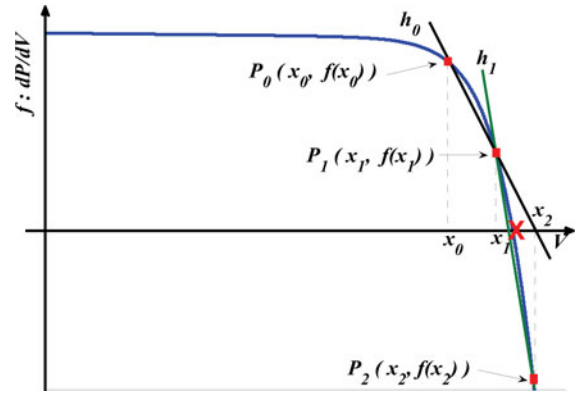
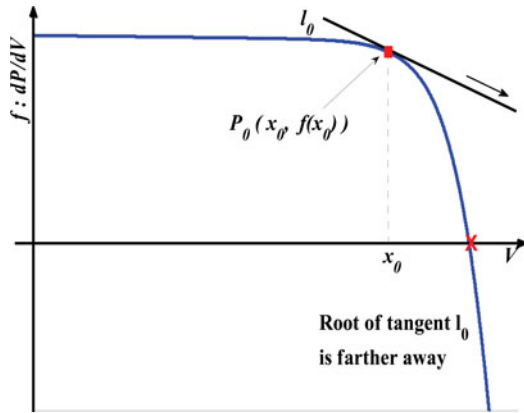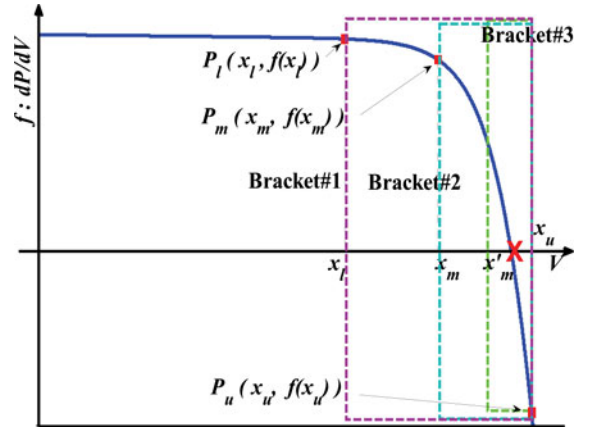Fig. 7.   NRM x^* is represented by the cross.

Fig. 8.   NRM (wrong initial value choice).

$f(x)$ at the point x_n. That is, $l_n(x_{n+1}) = 0$ with

$$l_n(x) = f'(x_n) \cdot (x - x_n) + f(x_n) \quad n = 0, 1, 2 \ldots . \quad (3)$$

This general process is represented in Fig. 7. The main advantage of the NRM is its fast convergence rate (order of convergence 2); fastest among all the methods considered here. However, the NRM has important disadvantages. An important one of those is that this method requires derivative values of the function at each instance, which adds computational complexity and increases the error in the solution. Another even more important disadvantage, exemplified in Fig. 8, is that the algorithm will not converge for most initial value choices in the first iteration to the left of the MPP. That is, only a very narrow interval of initial guesses will lead to a convergence to the MPP. Thus, in practical implementations, the NRM applied to MPPT is likely to diverge or to be numerically unstable.

2) Secant Method: The (secant method) SM exemplified in Fig. 9 is in many ways similar to the NRM. The SM is another iterative algorithm in which the fundamental equation is given by

$$x_{n+1} = x_n - f(x_n) \cdot \frac{x_n - x_{n-1}}{f(x_n) - f(x_{n-1})} \quad n = 0, 1, 2 \ldots . \quad (4)$$

For the SM, x_{n+1} is the root for a secant line $h_n(x)$ to the

Fig. 9.   Secant Method.

Fig. 10.   Bisection method.

function $f(x)$ at the point x_n such that $h_n(x_{n+1}) = 0$ with

$$h_n(x) = \frac{f(x_n) - f(x_{n-1})}{x_n - x_{n-1}} \cdot (x - x_n) + f(x_n)$$
$$n = 0, 1, 2 \ldots . \quad (5)$$

Like the NRM, convergence to a solution is not guaranteed with the SM. Also, the SM convergence rate has an order of 1.618, which is slightly slower than the NRM. Yet, in the SM there is no need to compute derivatives.

B. Bracketing Method

Instead of relying on point estimates for the root like in the open methods, bracketing methods are based on an interval defined by two points. In the next immediate analysis, two of the most popular bracketing methods and a newly proposed algorithm are discussed.

1) Bisection Method: The bisection method (BSM) algorithm, represented in Fig. 10, can be summarized in the following steps.

1) Given a well-defined function $f(x)$, choose a lower value x_l and an upper value x_u. These two points define an interval $[x_l, x_u]$ that must include the root x^* of $f(x)$. That is, $f(x)$ has opposing signs in x_l and x_u, e.g., $f(x_l)f(x_u) < 0$.
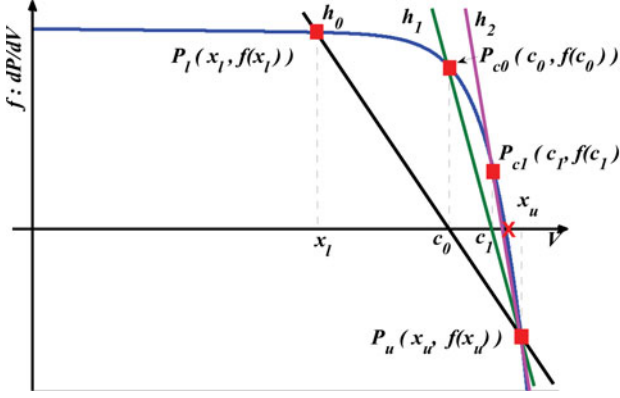
Fig. 11. Regula falsi method.

2) Approximate the root to the midpoint x_m of the interval $[x_l, x_u]$. That is

$$x_m = \frac{x_u + x_l}{2}. \tag{6}$$

3) If $f(x_l)f(x_m) < 0$, then set $x_u = x_m$ and repeat the previous step. If $f(x_l)f(x_m) > 0$, then set $x_l = x_m$ and repeat the previous step. If $|f(x_m)| \le \varepsilon$ (where ε is the tolerance), then take x_m as the root or approximation.

The BSM convergence rate is slower than the SM. Yet, with the BSM root convergence is guaranteed.

2) Regula Falsi Method: The regula falsi method (RFM) is a linearly convergent root-finding algorithm for continuous functions with one independent variable. It is a hybrid of the bisection search theorem (BST) [13] and the secant method [12]. A value c_i is derived from

$$c_i = \frac{x_l \cdot f(x_u) - x_u \cdot f(x_l)}{f(x_u) - f(x_l)}, \quad i = 0, 1, \ldots. \tag{7}$$

This found value c_i is then used to substitute the midpoint of each interval $[x_l, x_u]$ as the root approximation used in the BST method. This process is described in both the next algorithm and through Fig. 11.

1) Given a continuous function $f(x)$, find initial points x_l and x_u, such that $x_l \ne x_u$ and $f(x_l)f(x_u) < 0$. Hence, according to the intermediate value theorem, the root of $f(x)$ is located inside the interval $[x_l, x_u]$.
2) Calculate the approximate value for the root c_i with (7).
3) If $|f(c_i)| \le \varepsilon$ (where ε is the tolerance), then it is considered that the root has been reached and that c_i is the root. Else, if $f(c_i) \cdot f(x_u) < 0$, then let $x_l = c_i$; else if $f(c_i) \cdot f(x_l) < 0$, then let $x_u = c_i$. These changes yield a smaller interval.
4) Iterate steps (ii) and (iii) until the root is reached.

Although the RFM is only linearly convergent, it is generally faster than the BST method because the RFM utilizes the magnitude data of $f(x)$ at each point, which is unique for every different function $f(x)$ depending on its curvature whereas the BST method only uses the sign information of $f(x)$. As Fig. 11 suggests, the RFM leaves always one end point of the interval fixed, which generates an opportunity for improvement. In the RFM, root convergence is guaranteed as proved in [28].
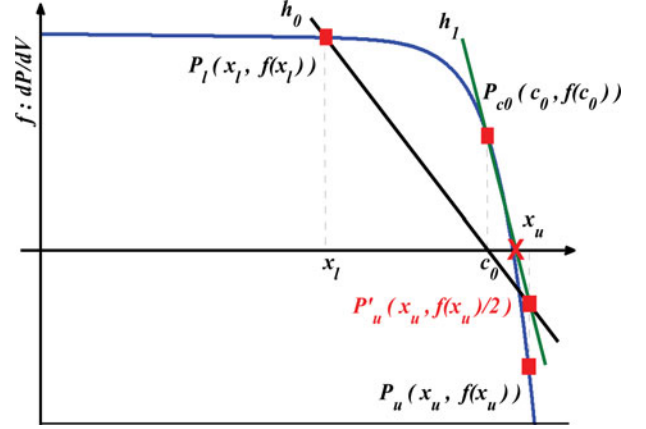

Fig. 12. Modified regula falsi method.

3) Modified Regula Falsi Method: As Fig. 11 indicates, for a convex or concave function $f(x)$, the RFM converges to the root slowly because one of the end points of the root search interval is fixed, resulting in a constant magnitude for $f(x)$ at that particular point. This problem is improved by the MRFM (see Fig. 12), introduced in a general theoretical context in [28]. The MRFM is similar to the RFM except that the following process replaces step 2) of the RFM:

2) If $f(x_l) \cdot f(x_u) < 0$ and $f(x_l) > 0$, then $f(x_u)$ is replaced in (7) by $f_p(x_u) = f(x_u)/2$ and $f_p(x_l) = f(x_l)$

$$c_i = \frac{x_l \cdot f_p(x_u) - x_u \cdot f_p(x_l)}{f_p(x_u) - f_p(x_l)} = \frac{x_l \cdot f(x_u) \cdot 0.5 - x_u \cdot f(x_l)}{0.5 \cdot f(x_u) - f(x_l)}. \tag{8}$$

If $f(x_l) \cdot f(x_u) < 0$ and $f(x_l) < 0$, then $f(x_l)$ is replaced in (7) by $f_p(x_l) = f(x_l)/2$ and $f_p(x_u) = f(x_u)$

$$c_i = \frac{x_l \cdot f_p(x_u) - x_u \cdot f_p(x_l)}{f_p(x_u) - f_p(x_l)} = \frac{x_l \cdot f(x_u) - x_u \cdot f(x_l) \cdot 0.5}{f(x_u) - 0.5 \cdot f(x_l)}. \tag{9}$$

That is, these changes effectively decrease the magnitude of $f(x)$ by 1/2 at one of the bracket ends in order to achieve faster convergence, as it is represented in Fig. 12. Mathematicians have investigated many variations in the RFM, some by coming up with different strategies on how much weight is put on the degrading factor or the retaining end point portion of the algorithm [29]–[32]. The MRFM is one of these variations and is known as the Illinois Method. These different options derived from the RFM are a potential area for additional research in order to increase the speed of convergence to the MPP, which are out of the scope of this work.

IV. ROOT-FINDING ALGORITHMS APPLICATION TO MPPT

This section discusses implementation of the aforementioned algorithms into DMPPT methods. Since the dP/dV curve of a PV panel is a well-defined concave function, a root that solves $dP/dV = 0$ always exists. Hence, practical implementation of the aforementioned root-finding algorithms in order to find the MPP implies that $f(x)$ needs to be replaced by dP/dV. Figs. 7–12 exemplified the concepts and also represented how the methods mentioned earlier are applied to an analog MPPT. Since this

study presents a new MPPT algorithm based on the MRFM, the focus of the analysis is on the MRFM. However, analogous conclusions can be simply drawn for other methods, too.

A. Digital Maximum Power Point Tracking

Since all the aforementioned methods are based on the assumption that the function $f(x)$—which in MPPT is replaced by dP/dV—for which the root is being sought is continuous, the analysis needs to examine what issues may arise when implementing those methods in a digital domain. These issues to consider when implementing DPPT of root-finding algorithms that are based on the assumption of continuity are algorithm numerical stability, sampling-generated error of an analog signal—i.e., the quantization error—and approximation of the value of a derivative in the digital domain—i.e., discretization error.

1) Numerical Stability: Each root-finding optimization method is based on a repetitive process of finding a new approximation to the root. In the past, limitation in the computation resources round-off errors and truncation errors critically affected the outcome of such an iterative process. However, technological advances in digital signal processing have made nowadays round-off and truncation errors to become negligible. When applying a root-finding method in a digital system, it is important for the algorithm to be numerically stable, i.e., it is proven to converge to a root. Proof of convergence of the root-finding methods mentioned in this paper is well known and for that reason they are not discussed in detail. Readers can find this detail analysis in textbooks, such as [28], in which proof of convergence is based on considering each new approximation as a monotonically increasing sequence, which is then compared within an interval, from where it is identified that the sequence has an upper bound, which proofs that the sequence converges.

2) Quantization Error: In a digital implementation of an MPPT algorithm, the voltage across the PV module V_{pv} and the current generated are sampled and processed by an analog-to-digital converter (ADC) that discretizes the analog signal or measurement to be processed in the digital domain. But a quantization error exists because of limited number of bits representing the measured or sampled value. The magnitude of the quantization error can range from 0 to half of the smallest resolution the ADC [5] which equals

$$\text{Quantization Error Maximum Magnitude} = \frac{1}{2} \cdot \frac{V_{p-p}}{2^N} \tag{10}$$

where V_{p-p} is the peak-to-peak measurement range of the signal and N is the ADC resolution bits. From (10), it is shown that the higher the resolution (N) of the ADC, the smaller the maximum error. But the finer the resolution of an ADC, the more expensive it becomes. Hence, there is a tradeoff between minimizing cost and quantization error. The quantization error can be minimized by decreasing the signal measurement range V_{p-p}. This can be achieved by using a voltage divider circuit to decrease the signal range and sending that measured signal to a low-voltage range ADC. The reduced signal value can then later be compensated through software programming to get the actual measured value before the voltage divider circuit. As was mentioned for the

round off and truncation errors, the quantization error issue can be ignored due to the continued decrease in the cost of high-resolution ADC. Presently, a 12- or 16-bit resolution ADC is embedded as peripherals on many common inexpensive DSPs, such as the TI TMS320F28335 DSP chip. With such an ADC resolution, it is possible to obtain errors of about 0.1 mV to 2 mV for a ±10 V range signal, which is sufficiently small to be ignored.

3) Discretization Error ($\vartheta_{x_0}(h)$): Digital implementation of MPPT algorithms requires addressing issues with computing the dP/dV derivative in the digital domain. Since a digital processor can only process discrete data samples, a true derivative at an operating point cannot be achieved without some error called discretization error, $\vartheta_{x_0}(h)$. In the MRFM method, a backward numerical differentiation quotient is used to approximate the derivative at an arbitrary operating point x_0. When a derivative at an operating point V_{x0} is needed, the backward difference quotient is found by immediately sampling another value ($V_{x_{0'}}$) separated from the operating point by a fixed small value ΔV. So, the value of the finite difference quotient at point x_0 is

$$\left.\frac{dP}{dV}\right|_{V=x_{0'}} \approx \frac{\Delta P}{\Delta V} = \frac{V_{x_0} \cdot I_{x_0} - V_{x_{0'}} \cdot I_{x_{0'}}}{V_{x_0} - V_{x_{0'}}} \tag{11}$$

where $V_{x_{0'}} = V_{x_0} - \Delta V$, and V_{x0}, I_{x0}, and $V_{x_{0'}}, I_{x_{0'}}$ are sampled voltages and current values at point x_0 and $x_{0'}$, respectively.

From the Taylor series representation of the derivative of a function, $g(x)$ can be represented as

$$g'(x_0) = \frac{g(x_0) - g(x_0 - h)}{h} - \frac{g''(x_0) \cdot h^2}{2!} - \frac{g'''(x_0) \cdot h^3}{3!} - \cdots$$

$$= g'_e(x_0) - \frac{g''(x_0) \cdot h^2}{2!} - \frac{g'''(x_0) \cdot h^3}{3!} - \cdots \tag{12}$$

where h is the difference between x_0 and $x_{0'}$ equivalent to ΔV in (11), and $g'_e(x_0)$ denotes the estimated derivative value equivalent to $\Delta P/\Delta V$ in (11). That is, $g(x)$ is analogous to the function $P(V)$. Then, the error between the true derivative and the estimated value is

$$\vartheta_{x_0}(h) = g'(x_0) - g'_e(x_0) = -\frac{g''(x_0) \cdot h^2}{2!}$$

$$- \frac{g'''(x_0) \cdot h^3}{3!} - \cdots. \tag{13}$$

In (13), it is shown that a sufficient value for h—analogous to ΔV in a practical MPPT implementation— between two sample points must be chosen to approximate a derivative value that has a small error $\vartheta_{x_0}(h)$. Yet, h must also be large enough to provide a valid sample value in a noisy measurement environment. In doing so, the value of h and the corresponding discretization error $\vartheta_{x_0}(h)$generated by h must meet a specified tolerance range defined by the system designer.

As mentioned earlier, all root-finding algorithms have a termination condition given by the tolerance for the searched root value. In the proposed MRFM, when implemented digitally, the tolerance was set to reach the MPP within 99.9% of its given value at the predetermined lowest irradiance condition. For the analysis, the lowest irradiance was chosen to be at $200 \, \text{W/m}^2$. This irradiance condition was chosen for the MPPT algorithm
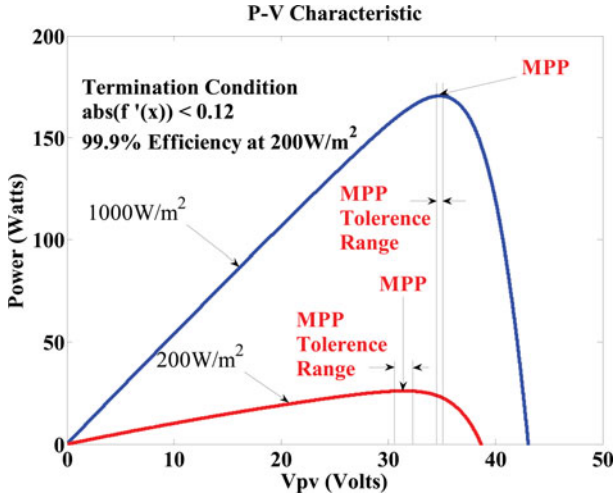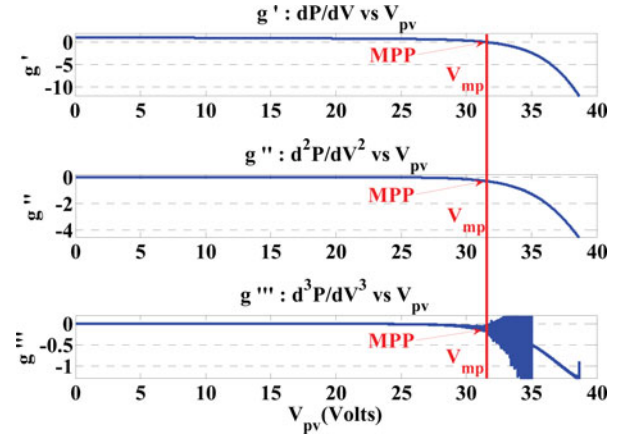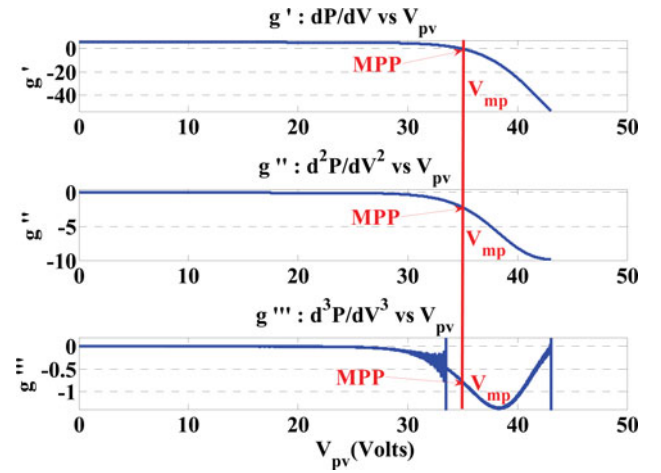
Fig. 13. Termination condition comparison between two irradiance levels.

Fig. 14. dP/dV, d^2P/dV^2, and d^3P/dV^3 of PV module at 200 W/m^2, 25 °C.

Fig. 15. dP/dV, d^2P/dV^2, and d^3P/dV^3 of PV module at 1000 W/m^2, 25 °C (STC).

design because for a fixed termination condition, as the irradiance increases, the operating point range that meets the objective of falling within 99.9% of the MPP decreases (see Fig. 13). Hence, if a high irradiance condition is chosen as the reference for specifying the tolerance, when the irradiance decreases from the reference level, it is possible to find termination conditions that are beyond the 99.9% of the MPP. In the particular examples used in this paper, another advantage of selecting 200 W/m^2 as the reference irradiance level for the tolerance is that at this irradiance level $I_{sc} \approx 1$ A. From the simulation data in Fig. 13 of the dP/dV versus V curve, the termination condition is $|f(x_n)| \leq 0.12$. This value corresponds to an interval of $\Delta V = 0.4$ V around the MPP. This voltage difference is the error bound or accuracy tolerance considered in practical cases studied in this paper.

A low cost—less than a hundred dollars—digital MPP tracker can be realized with an inexpensive microcontroller that is still fast enough to run each step of the DMPPT algorithm within each sampling period (in the order of a millisecond), and an ADC with a resolution that depends on the input signal range—yet, most DSP chips have this function already embedded. Evidently, a power electronic converter with a DPWM controlled needs to be added. In this study, a boost converter was chosen because it is simple and widely used for this application. However, the analysis can easily be extended to other dc–dc converters that can be used as power electronic interfaces for such systems. When the dc–dc converter is connected to a battery or a constant voltage load, the output voltage of the converter is fixed. This is another assumption also considered in this study because batteries are often used in sustainable PV systems in order to power the load when there is not enough sunlight. The assumed constant output voltage is $V_{out} = 48$ V. A microcontroller running the MPPT algorithm takes the discretized voltage and current values and generates a DPWM duty cycle D that regulates the converter input voltage V_{pv}. V_{pv} is the voltage across the PV module. In the case of the boost converter used here, if the duty cycles D_1 and D_2 correspond to input voltages V_{pv1}, and V_{pv2}, respectively, and assuming $V_{pv1} < V_{pv2}$, $D_1 > D_2$, then $\Delta V = V_{pv2} - V_{pv1}$,

and $\Delta D = D_1 - D_2$. Thus,

$$\Delta D = \frac{\Delta V}{V_{out}} \rightarrow \Delta V = \Delta D \cdot V_{out}. \quad (14)$$

From the definition of a derivative and from (12) and (13), the smaller the value of h, the closer the approximate value of a derivate to its true value. Mathematically, with continuous variables and functions, there is no direct limitation in h (equivalent to ΔV in (14)). However, in digital implementation of (11), ΔV in (14) is affected by the limited resolution of the DPWM. Hence, the resolution of the DPWM becomes the deciding factor when selecting ΔV. The smallest resolution of a DWPM is referred to as a tick or LSB and this will be a lower bound for ΔV. In the experimental setup here, 1 tick is 25 ns which is $\Delta D = 0.00125$ for a 50 kHz switching frequency DPWM signal and from $V_{out} = 48$ V, (14) corresponds to $h = \Delta V = 0.06$ V.

In (13), $\vartheta_{x_0}(h)$ depends on $g''(x_0)$, $g'''(x_0)$, and h—i.e., d^2P/dV^2, d^3P/dV^3, and ΔV. The possible range of values for $g''(x_0)$ and $g'''(x_0)$ are shown in Figs. 14 and 15 for solar irradiances of 200 W/m^2 and 1000 W/m^2, respectively. Consider a worst case scenario when $g''(x_0)$ and $g'''(x_0)$ have their largest value—i.e., when the irradiance is 1000 W/m^2. In Fig. 15,

TABLE I
PARAMETER VALUES FOR DIFFERENT TICK VALUES

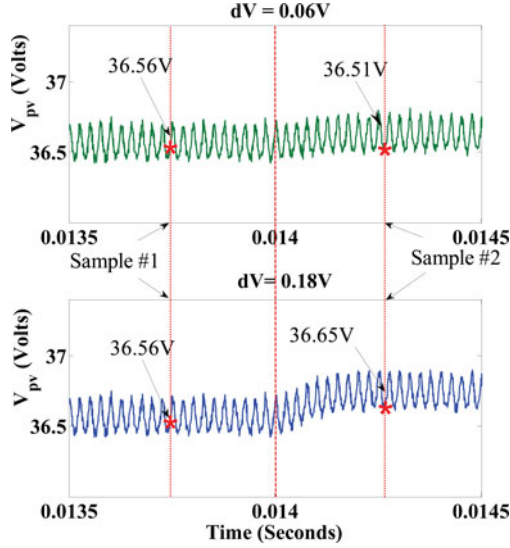| Ticks	ΔD	h equivalent to ΔV	$\frac{h^2}{2}$	$\max\left|\frac{g''h^2}{2}\right|$	$\frac{h^3}{3!}$	$\max\left|\frac{g'''h^3}{6}\right|$
1 ticks	0.0012	0.06	0.0018	0.018	0.00003	0.000054
2 ticks	0.0025	0.12	0.0072	0.072	0.00028	0.000432
3 ticks	0.0037	0.18	0.0162	0.162	0.00097	0.001458
4 ticks	0.005	0.24	0.0288	0.288	0.00230	0.003456
5 ticks	0.0062	0.3	0.045	0.45	0.0045	0.00675

Fig. 16.   Error caused by a small ΔV value.

the range for $g'(x_0)$, $g''(x_0)$, and $g'''(x_0)$ are $-54 < g'(x_0) < 5.5$, $-10 < g''(x_0) < -0.01$, and $-1.37 < g'''(x_0) < 0$, respectively. Considering these values and the calculations indicated in Table I, the third-order term of the discretization error ($\vartheta_{x_0}(h)$) has a significantly small value ranging from 0.000054 to 0.00675. This range of values is less than 0.01, so the third-order term in (13) can be ignored. Thus, the only significant term that needs to be considered is the second-order term, so (13) becomes

$$\vartheta_{x_0}(h) \approx -\frac{g''(x_0) \cdot h^2}{2!}. \tag{15}$$

Once again, from (15), ideally the smaller the h (or ΔV), the closer it is to its derivative true value at a given point. However, due to ambient EMI noise, switching noise of the dc–dc converter, and quantization errors mentioned earlier, a value of ΔV or h too small may cause errors to occur during data acquisition. This is illustrated in Fig. 16 which shows two sampling instances before and after a duty cycle change for two different cases. The first is for 1 tick ($\Delta V = 0.06$ V) and the second is for 3 ticks ($\Delta V = 0.18$ V). For the former case, it is shown that although the value for ΔV is small and decreases $\vartheta_{x_0}(h)$ the most, the step size is too small to overcome the effects of noise. Hence, an error occurs when sampling, whereas for the latter case the sampled values for the two instances are sufficient. Thus, an upper bound of h—i.e., ΔV— is also needed in order to complete the sampling portion of the controller design. In short, h (or ΔV) must be a value small enough to keep $\vartheta x_0(h)$ small but large enough so that the controller is robust against noise actions.

Thus, in order to choose the interval h for the proposed method (e.g., the MRFM), one more criteria need to be considered. From the MRFM algorithm, at each iteration the new approximation of the root is once again from (8) and (9)

$$c_n = \frac{a_n f_p(b_n) - b_n f_p(a_n)}{f_p(b_n) - f_p(a_n)} = \frac{a_n g'_p(b_n) - b_n g'_p(a_n)}{g'_p(b_n) - g'_p(a_n)} \tag{16}$$

where a_n and b_n are the lower and upper bounds of an interval bracket $[a_n, b_n]$, also the subscript p indicates that the function $f(x)$ follows the condition mentioned in (8) and (9). The true value is denoted c_n^{true} and the estimation value affected by the approximation of the derivative or discretization error is c_n^{est} which is given by

$$c_n^{\text{est}} = \frac{a_n g'_{e,p}(b_n) - b_n g'_{e,p}(a_n)}{g'_{e,p}(b_n) - g'_{e,p}(a_n)}. \tag{17}$$

Hence, from (13) and (16)

$$
\begin{aligned}
c_b^{\text{true}} &= \frac{a_n g'_p(b_n) - b_n g'_p(a_n)}{g'_p(b_n) - g'_p(a_n)} \\
&= \frac{a_n g'_{e,p}(b_n) - b_n g'_{e,p}(a_n) + \vartheta_{p,b_n}(h) \cdot a_n - \vartheta_{p,a_n}(h) \cdot b_n}{g'_{e,p}(b_n) - g'_{e,p}(a_n) + \vartheta_{p,b_n}(h) - \vartheta_{p,a_n}(h)}.
\end{aligned}
\tag{18}
$$

Since from Fig. 15, the value of $g''(x)$ for the minimum voltage value is approximately 0 V and the value of $g''(x)$ for the maximum voltage value is approximately -10 V, from (15) and assuming that b_n is the retaining point

$$
\begin{aligned}
\vartheta_{p,b_n}(h) - \vartheta_{p,a_n}(h) &\approx -\frac{g''_p(b_n) \cdot h^2}{2!} + \frac{g''_p(a_n) \cdot h^2}{2!} \\
&= \frac{h^2}{2}(g''_p(a_n) - g''_p(b_n)) = \frac{h^2}{2}\left(g''(a_n) - \frac{g''(b_n)}{2}\right) \\
&< \left(0 - \frac{-10}{2}\right)\frac{h^2}{2} < 5\frac{h^2}{2}.
\end{aligned}
\tag{19}
$$

Fig. 15 also indicates that $-54 < g'(x_0) < 5$. Thus, from (19) $g'_{e,p}(b_n) - g'_{e,p}(a_n) \gg \vartheta_{b_n}(h) - \vartheta_{a_n}(h)$. Therefore, $\vartheta_{b_n}(h) - \vartheta_{a_n}(h)$ can be ignored in the denominator of (18), so with the help of (17), (18) now becomes

$$
\begin{aligned}
c_n^{\text{true}} &= \frac{a_n g'_{e,p}(b_n) - b_n g'_{e,p}(a_n) + \vartheta_{p,b_n}(h) \cdot a_n - \vartheta_{p,a_n}(h) \cdot b_n}{g'_{e,p}(b_n) - g'_{e,p}(a_n)} \\
&= c_n^{\text{est}} + \varepsilon(h)
\end{aligned}
\tag{20}
$$

where $\varepsilon(h)$ is the error between c_n^{true} and c_n^{est}. Hence,

$$
\begin{aligned}
\varepsilon(h) &= \frac{\vartheta_{p,b_n}(h) \cdot a_n - \vartheta_{p,a_n}(h) \cdot b_n}{g'_{e,p}(b_n) - g'_{e,p}(a_n)} \\
&= \frac{h^2}{2}\left(g''_p(a_n) \cdot b_n - g''_p(b_n) \cdot a_n\right)\frac{1}{g'_{e,p}(b_n) - g'_{e,p}(a_n)} \\
&= \frac{h^2}{2}\frac{\left(g''_p(a_n) \cdot (a_n + \Delta_{Vn}) - g''_p(a_n + \Delta_{Vn}) \cdot a_n\right)}{g'_{e,p}(a_n + \Delta_{Vn}) - g'_{e,p}(a_n)}
\end{aligned}
\tag{21}
$$

where Δ_{Vn} is $b_n - a_n$. From (21) as $V_n \to 0$, $\varepsilon(h) \to 0$, which means as the iterative process of the MRFM continues, the bracket size decreases resulting in $c_n^{\text{true}} \approx c_n^{\text{est}}$. Thus, both the bracket size Δ_{Vn} and the error $\varepsilon(h)$ are the maximum for the initial bracket. For the MRFM [22], the initial bracket size Δ_{V0} is 4 V. This value for Δ_{V0} is somewhat arbitrary as Δ_{V0} could take any value up to V_{oc}. In this case, it was considered about ten times the tolerance and one tenth of V_{oc}. Next, h that minimizes $\varepsilon(h)$ needs to be found. Assuming that b_n is the retaining point, (21) becomes

$$\varepsilon(h) = \frac{h^2}{2} \frac{(g''(a_n) \cdot (a_n + \Delta_{v_n}) - (g''(a_n + \Delta_{v_n})/2) \cdot a_n)}{(g'_e(a_n + \Delta_{v_n})/2) - g'_e(a_n)}$$

$$< 5 \cdot \frac{h^2}{2}. \tag{22}$$

To sum up, a value h needs to be chosen so that (15), (19), and (22) are small enough so they meet the tolerance condition of $\Delta V = 0.4$ V and so that $| g'(x_n)| \leq 0.12$. Yet, h needs to be large enough to be robust against noise effects. In the experimental setup detailed in the next section, the noise amplitude was measured to be 130 mV peak to peak, so $h = 0.18$ V was the smallest value large enough to overcome the effects of the noise. When $h = 0.18$ V is used in (19) and (22) and considering from Fig. 16 that $g'(x)$ can take values between -54 and 5.5, it can be concluded that in order to approximate the derivative at a point $h = 0.18$ V is a sufficiently good value representing the length of an interval given by two samples. Hence, in the practical application discussed next, when calculating derivatives from (11), ΔV is considered equal to 0.18 V.

V. SIMULATION-BASED COMPARISON

A simulated comparison was initially explored in order to verify the root-finding methods for DMPPT. The arguable two most popular DMPPT methods—the P&O and the INC methods—are also considered. The P&O method is widely used due to its implementation simplicity but the operating point constantly oscillates around the MPP resulting in loss of energy. The other popular method is the INC method, which has a fixed step size that often leads to trade offs associated with the step size choice: if the step size is large, the MPP is reached faster than when a small step size is chosen. But accuracy of large step sizes is worse than that of small step sizes. Simulation results performed at STC for different root-finding algorithms are shown in Fig. 17. Hence, the MPP is reached, when V_{pv} equals $V_{\text{mp}} = 34.8$ V. The plots in Fig. 17 indicate that the SM takes 6 steps to reach the MPP, the BSM 14 steps, the RFM 10 steps, and the MRFM 6 steps. Hence, these results confirm not only that the different root-finding algorithms mentioned in this paper can be used as DMPPT algorithms (for the NRM, SM, when the initial conditions are good) but also that the MRFM is the fastest method in tracking the MPP. As Fig. 17 displays, digitally implemented SM DMPP is fast and accurate but only when the initial point is near the MPP. However, when the initial point is far from the MPP, the SM diverges. The NRM was not simulated because it has similar behavior to the SM but it is more complex to implement due to the need to calculate the second deriva-
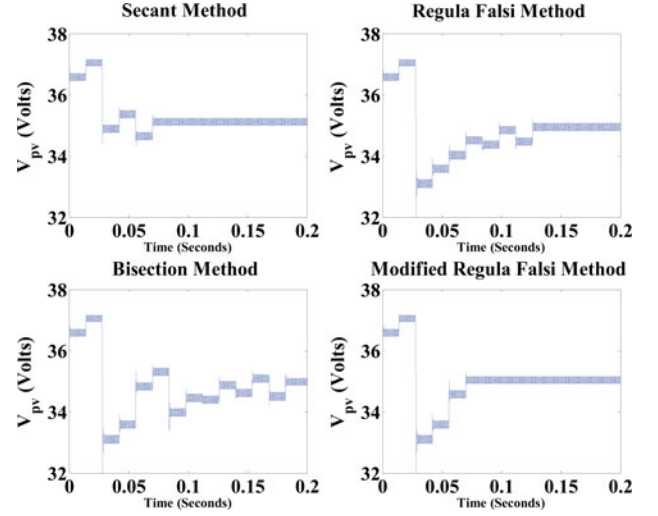

Fig. 17. Comparison of the Root-Finding Methods' DMPPT through simulations.

Fig. 18. Boost converter circuit with a PV module as a source.

tive. Hence, although the NRM is the fastest method discussed earlier here, due to the complication of calculating the second derivative and the aforementioned instability issues, it is not a good choice as a MPPT algorithm. The next three aforementioned bracketing methods solve the instability issue of the SM and the NRM and are shown in Fig. 17. As was discussed earlier and Fig. 17 shows, the DMPPT BSM implemented guarantees to find the MPP but it is slow compared to the RFM and MRFM in finding the MPP. As Fig. 17 also displays, the RFM is faster than the BSM and as it was discussed in the previous section it also guarantees to reach the MPP. However, as Fig. 17 shows, the MRFM is fastest of all discussed methods that guarantee convergence to the MPP. It reaches the MPP immediately after finding a bracketing interval. Moreover, compared with a fixed step size algorithm (e.g., P&O and INC), the proposed MRFM is more accurate because in the MRFM the step size varies while approaching the MPP, whereas in fixed step cases, oscillation occurs around the true MPP.

VI. EXPERIMENTAL SETUP AND RESULTS

A. Experiment setup

Experiments were conducted with a Sharp NE-170U1 PV module under solar light in order to validate the analysis. The basic specification of this PV module is $V_{\text{oc}} = 43.2$ V, $I_{\text{sc}} = 5.47$ A, and $P_{\text{max}} = 170$ W at $V_{\text{mp}} = 34.8$ V, $I_{\text{mp}} = 4.90$ A. A boost converter was chosen to interface the PV module and to implement MPPT because of its simplicity and because boost-type

Fig. 19.   DMPPT experimental setup for DMPPT.

Fig. 20.   DPWM signal from the FPGA.

converter is a common choice to interface PV modules in practical applications. The boost converter is operated in continuous conduction mode (CCM) and the circuit parameters corresponding to the circuit schematic in Fig. 18 are $L = 300\ \mu$H, $C_2 = 1500\ \mu$F, and PV input Capacitor $C_1 = 10\ \mu$F, with a switching frequency of 50 kHz. The inductance value was chosen to keep the converter operating in the CCM even during low irradiance conditions when I_{in} is minimal. According to [34]

$$L > \frac{V_{\text{in}}}{2 I_{\text{in}} f} \qquad (23)$$

As mentioned in Section IV, a low-cost digital MPP tracker can be commercially realized with an inexpensive microcontroller, an ADC, and a DPWM controlled boost converter. However, due to the prototyping nature of this project, an NI CompactRIO (cRIO) system platform was used as shown in Fig. 19 because it provides more flexibility and implementation ease, particularly when control parameters need to be continuously changed. The voltage and current values were acquired through an NI 9215 Analog Input Output (AIO) Module into a standard computer from where they were captured. This AIO module has a 16-bit ADC with a signal range of ±10 V. The control DPWM signal is generated by the field programmable gate array (FPGA) in the cRIO and it is output through an NI 9401 Digital Input Output (DIO) Module. The FPGA uses an internal clock of 40 MHz to generate a tick every 25 ns and produces a DPWM signal as shown in Fig. 20. Thus, an 800 tick duration is required in order to generate a 50-kHz DPWM signal. The "on" or "high" ticks are related to the duty cycle through

Fig. 21.   Experimentally generated results for the P&O DMPPT.

$$k = \lceil 800D \rceil \qquad (k : \text{Number of High ticks for Duty Cycle } D). \qquad (24)$$

B. Experimental Results

Figs. 21–27 show the experimental results obtained for all of the root-finding optimization methods mentioned in this paper. Each figure has two parts. The left side of each of these figures consists of the DMPPT algorithm tracking the MPP, i.e., it indicates real extracted power. On the right side, they show an I–V sweep done immediately after the tracking to verify the true MPP, i.e., it indicates real PV panel MPP. These experimental results follow the simulation outputs discussed in Section VI-A very closely. Figs. 21–23 show the experimental results of the P&O and INC methods. Figs. 22 and 23 show the INC method at two different duty cycle step settings. Fig. 22 is set at a large duty cycle step ($\Delta D = 0.01$) in order to show that it oscillates

Fig. 22. Experimentally generated results for the INC DMPPT, $\Delta D = 0.01$.

Fig. 23. Experimentally generated results for the INC DMPPT, $\Delta D = 0.005$.
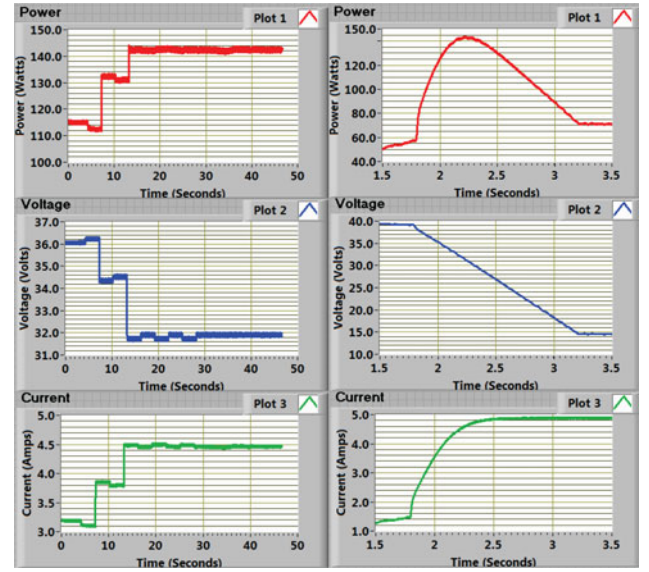

Fig. 24. Experimentally generated results for the SM DMPPT.

Fig. 25. Experimentally generated results for the BSM DMPPT.

Fig. 26. Experimentally generated results for the RFM DMPPT.

around the MPP, whereas Fig. 23 displays the case of a small duty cycle step ($\Delta D = 0.005$) which takes longer to converge to the vicinity of the MPP. Fig. 24 exemplifies the SM with a good initial condition choice. As shown, the SM reaches the MPP in five sets of sample. One set consists of two samples to calculate the backward difference quotient. Fig. 25 depicts the BSM. For this method, the MPP is reached in a total of eight sets. Fig. 25 exemplifies the RFM which requires a total of five sets to reach the MPP. Finally, Fig. 27 shows the MRFM. This newly proposed MPPT method is the fastest of all of those tested here, reaching the MPP in a total of four sets. Therefore, experiments validate the analysis showing not only convergence to the MPP for the discussed root-finding methods, but also that the newly proposed method based on the MRFM converges to the MPP faster than all other methods with ensured convergence to the MPP.

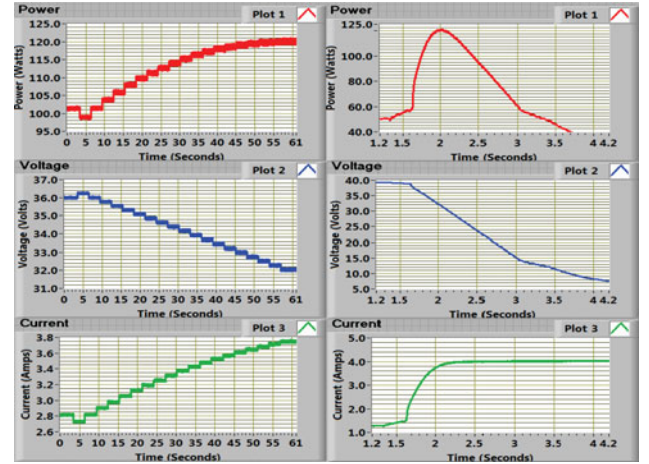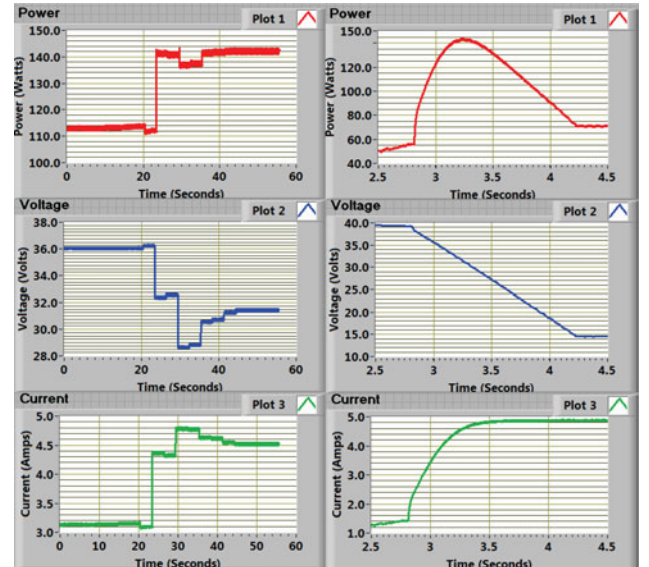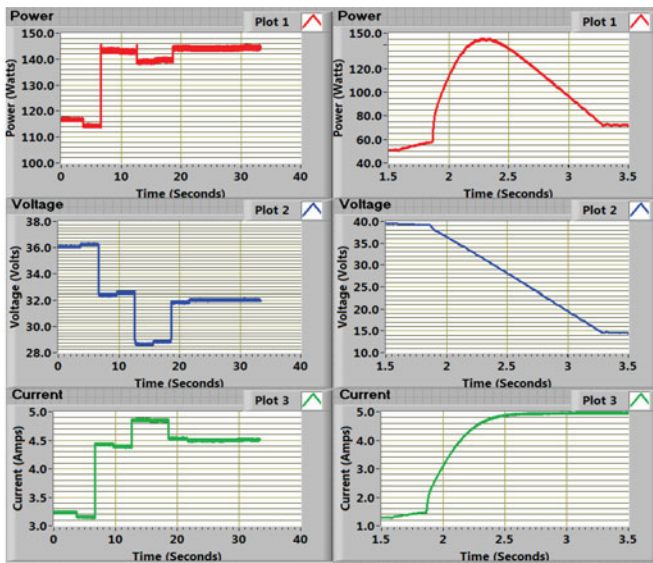Fig. 27.   Experimentally generated results for the MRFM DMPPT.

VII. CONCLUSION

Photovoltaic systems are one of the leading technologies envisioned in order to achieve carbon footprint reduction and more sustainable energy generation means. In these systems, power electronic interfaces are essential components because they allow the necessary energy efficiency conversion to harness this renewable energy source. Hence, MPPT methods are key enablers of a more energy sustainable society. Due to their implementation ease, low cost, and flexible operation, in the past few years more and more controllers for such sustainable systems are being implemented on a digital platform. This paper has discussed an alternative perspective to the classical approach to MPPT. A numerical analysis approach for finding a root for the dP/dV function was performed. In particular, this paper comprehensively discussed classical root-finding algorithms and their use for MPPT was verified. Since these methods had been originally developed in a continuous variable domain, this study included thorough mathematical analysis that validates their implementation in a digital domain. This mathematical analysis discussed the impact of digitalizing such control strategies in terms of convergence to the MPP by exploring numerical stability characteristics of the root-finding methods in the digital domain and the effect of quantization and discretization errors. Based on the analysis, a new variable step DMPPT method called the MRFM was presented and its implementation was discussed. The analysis was validated both with simulations and with a hardware-based experimental test bed. All of the experiments were performed with the same test bed. No hardware alteration was needed in order to implement each method which in addition of highlighting a merit of digital implementation also ensures uniformity and unbiased testing for all discussed methods. These evaluations confirm the analysis by demonstrating that digitally implemented classical root-finding MPPT operates as expected. Bracketed methods are identified to be better options than open interval methods because in the latter conver-

gence to the MPP is not ensured. Simulations and experiments also confirm that the proposed MRFM seems to be fastest of the discussed algorithms to reach the MPP.

REFERENCES

[1] *World Energy Outlook 2009*. International Energy Agency, Nov. 10, 2009.

[2] *American Energy: The Renewable Path to Energy Security*: Worldwatch Institute, Sep. 2006. [Online]. Available: http://www.worldwatch.org/files/pdf/AmericanEnergy.pdf

[3] R. Wiser, M. Bolinger, P. Cappers, and R. Margolis, "Letting the sun shine on solar costs: An empirical investigation of photovoltaic cost trends in California," (Jan. 2006). [Online]. Available: http://eetd.lbl.gov/ea/ems/reports/59282.pdf

[4] T. Esram and P. Chapman, "Comparison of photovoltaic array maximum power point tracking techniques," *IEEE Trans. Energy Convers.*, vol. 22, no. 2, pp. 439–449, Jun. 2007.

[5] S. Busso and P. Mattavelli, *Digital Control in Power Electronics*. San Rafael, CA: Morgan & Claypool Publishers, 2006.

[6] J. W. Kimball and P. T. Krein, "Discrete-time ripple correlation control for maximum power point tracking," *IEEE Trans. Power Electron.*, vol. 23, no. 5, pp. 2353–2362, Sep. 2008.

[7] F. Liu, S. Duan, F. Liu, B. Liu, and Y. Kang, "A variable step size INC MPPT method for PV systems," *IEEE Trans. Ind. Electron.*, vol. 55, no. 7, pp. 2622–2008, Jul. 2008.

[8] B. Shen, B. Mwinyiwiwa, Y. Zhang, and B.-T. Ooi, "Sensorless maximum power point tracking of wind by DFIG using rotor position phase lock loop (PLL)," *IEEE Trans. Power Electron.*, vol. 24, no. 4, pp. 942–951, Apr. 2009.

[9] R.-Y. Kim, J.-S. Lai, B. York, and A. Koran, "Analysis and design of maximum power point tracking scheme for thermoelectric battery energy storage system," *IEEE Trans. Ind. Electron.*, vol. 56, no. 9, pp. 3709–3716, Sep. 2009.

[10] E. Koutroulis, K. Kalaitzakis, and N. C. Voulgaris, "Development of a microcontroller-based, photovoltaic maximum power point tracking control system," *IEEE Trans. Power Electron.*, vol. 16, no. 1, pp. 46–54, Jan. 2001.

[11] C. Hua, J. Lin, and C. Shen, "Implementation of a DSP-controlled photovoltaic system with peak power tracking," *IEEE Trans. Ind. Electron.*, vol. 45, no. 1, pp. 99–107, Feb. 1998.

[12] C. R. Sullivan and M. J. Powers, "A high-efficiency maximum power point tracker for photovoltaic arrays in a solar-powered race vehicle," in *Proc. IEEE Power Electron. Spec. Conf.*, Jun. 1993, pp. 574–580.

[13] H. D. Maheshappa, J. Nagaraju, and M. V. Krishna Murthy, "An improved maximum power point tracker using a step-up converter with current locked loop," *Renewable Energy*, vol. 13, no. 2, pp. 195–201, Feb. 1998.

[14] M. A. S. Masoum, H. Dehbonei, and E. F. Fuchs, "Theoretical and experimental analyses of photovoltaic systems with voltage and current based maximum power-point tracking," *IEEE Trans. Energy Convers.*, vol. 17, no. 4, pp. 514–522, Dec. 2002.

[15] Z. Salameh, F. Dagher, and W. Lynch, "Step-down maximum power point tracker for photovoltaic systems," *Solar Energy*, vol. 46, no. 5, pp. 279–282, 1991.

[16] N. Femia, G. Petrone, G. Spagnuolo, and M. Vitelli, "Perturb and observe MPPT technique robustness improved," in *Proc. IEEE Int. Symp. Ind. Electron.*, May 2004, vol. 2, pp. 845–852.

[17] N. Femia, G. Petrone, G. Spagnuolo, and M. Vitelli, "Optimization of perturb and observe maximum power point tracking method," *IEEE Trans. Power Electron.*, vol. 20, no. 4, pp. 963–973, Jul. 2005.

[18] K. H. Hussein, I. Muta, T. Hoshino, and M. Osakada, "Maximum photovoltaic power tracking: An algorithm for rapidly changing atmospheric conditions," *Proc. Inst. Elect. Eng.,* Jan. 1995, vol. 142, pt. G, no. 1, pp. 59–64.

[19] W. Xiao and W. G. Dunford, "A modified adaptive hill climbing MPPT method for photovoltaic power systems," in *Proc. IEEE 35th Annu. Power Electron. Spec. Conf.*, Jun. 2004, vol. 3, pp. 1957–1963.

[20] F. Luo, P. Xu, Y. Kang, and S. Duan, "A variable step maximum power point tracking method using differential equation solution," in *Proc. 2nd IEEE Conf. Ind. Electron. Appl.*, May 2007, pp. 2259–2263.

[21] W. Peng, H. Zhu, W. Shen, F. H. Choo, P. C. Loh, and K. K. Tan, "A novel approach of maximizing energy harvesting in photovoltaic systems based on bisection search theorem," in *Proc. IEEE Appl. Power Electron. Conf. Exp.*, 2010, pp. 2143–2148.

[22] S. Chun and A. Kwasinski, "Modified regula falsi optimization method approach to digital maximum powerpoint tracking for photovoltaic

application," presented at the Applied Power Electron. Conf. Expo., Fort Worth, TX, Mar. 6–10, 2011.

[23] T. Shimizu, M. Hirakata, T. Kamezawa, and H. Watanabe, "Generation control circuit for photovoltaic modules," *IEEE Trans. Power Electron.*, vol. 16, no. 3, pp. 293–300, May 2001.

[24] A. Kwasinski, "Identification of feasible topologies for multiple-input dc–dc converters," *IEEE Trans. Power Electron.*, vol. 24, no. 3, pp. 856–861, Mar. 2009.

[25] A. Khaligh, J. Cao, and Y.-J. Lee, "A multiple-input DC–DC converter topology," *IEEE Trans. Power Electron.*, vol. 24, no. 3, pp. 862–868, Mar. 2009.

[26] Y. Li, X. Ruan, D. Yang, F. Liu, and C. K. Tse, "Synthesis of multiple-input DC/DC converters," *IEEE Trans. Power Electron.*, vol. 25, no. 9, pp. 2372–2385, Sep. 2010.

[27] M. G. Villalva, J. R. Gazoli, and E. R. Filho, "Comprehensive approach to modeling and simulation of photovoltaic arrays," *IEEE Trans. Power Electron.*, vol. 25, no. 5, pp. 1198–1208, May 2009.

[28] L. R. Burden and J. D. Faires, *Numerical Analysis*. Boston: PWS-Kent, 1989 ISBN 0-534-93219-3.

[29] J. Naghipoor, S. A. Ahmadian, and A. R. Soheili, "An improved regula falsi method for finding simple zeros of nonlinear equations," *Appl. Math. Sci.*, vol. 2, no. 8, pp. 381–386, 2008.

[30] M. Dowell and P. Jarratt, "The Pegasus method for computing the root of an equation," *BIT*, vol. 12, pp. 503–508, 1972.

[31] R. F. King, "An improved Pegasus method for root finding," *BIT*, vol. 13, pp. 423–427, 1973.

[32] M. Dowell and D. Jarratt, "A modified regula falsi method for computing the root of an equation," *BIT*, vol. 11, no. 2, pp. 168–174, 1991.

[33] Texas Instruments Inc. *Application Report*, "Voltage mode boost converter small signal control loop analysis using the TPS61030," TI Literature Number SLVA274A.

[34] P. T. Krein, *Elements of Power Electronics*. New York, NY: Oxford Univ. Press, 1998.

Alexis Kwasinski (S'03–M'07) received the B.S. degree in electrical engineering from the Buenos Aires Institute of Technology (ITBA), Buenos Aires, Argentina, the Graduate Specialization degree in telecommunications from the University of Buenos Aires, Buenos Aires, in 1997, and the M.S. and Ph.D. degrees in electrical engineering from the University of Illinois at Urbana-Champaign, Champaign, in 2005 and 2007, respectively.

From 1993 to 1997, he was with the Telefónica, Argentina, for four years designing and planning telephony outside plant networks. Then, he was with Lucent Technologies Power Systems (later Tyco Electronics Power Systems) for five years as a Technical Support Engineer and a Sales Technical Consultant in Latin America. For three years, he was also a Part-time Instructor in charge of ITBA's Telecommunications Laboratory. He is currently an Assistant Professor in the Department of Electrical and Computer Engineering, The University of Texas at Austin, Austin. His current research interests include power electronics, distributed generation, renewable and alternative energy, and analysis of the impact of natural disasters on critical power infrastructure.

Dr. Kwasinski was a member of the Executive Committee of the Argentine Electrotechnical Association in 1994 and 1995. In 2005, he was the recipient of the Joseph J. Suozzi INTELEC Fellowship, and in 2007, he received the best technical paper award at INTELEC. In 2009, he received the National Science Foundation CAREER Award.

Seunghyun Chun (S'10) was born in Seoul, Korea, on August 26, 1975. He received the B.S. degree from Yonsei University, Seoul, in 2002, and the M.S. degree from the University of Southern California, Los Angeles, in 2004, both in electrical engineering. He is currently working toward the Ph.D. degree in electrical engineering at The University of Texas at Austin, Austin.

In August 2011, he became an Associate Professor in the School of Engineering, California Baptist University, Riverside. His current research interests include power electronics, digital control of dc–dc converters for renewable energy applications, smart grid, and engineering education.